



Nano- and Submicron Particles Emission during Gas Tungsten Arc Welding (GTAW) of Steel: Differences between Automatic and Manual Process

Elena Baracchini¹, Carlotta Bianco¹, Matteo Crosera¹, Francesca Larese Filon²,
Elena Belluso^{3,4,5}, Silvana Capella^{3,4}, Giovanni Maina⁶, Gianpiero Adami^{1*}

¹ *Dipartimento di Scienze Chimiche e Farmaceutiche, Università di Trieste, 34127 Trieste, Italy*

² *Unità Clinica Operativa di Medicina del Lavoro, Dipartimento Universitario Clinico di Scienze Mediche Chirurgiche e della Salute, Università di Trieste, 34129 Trieste, Italy*

³ *Dipartimento di Scienze della Terra, Università di Torino, 10125 Torino, Italy*

⁴ *Centro Interdipartimentale per lo Studio degli Amianti e di altri Particolati Nocivi "G. Scansetti", 10125 Torino, Italy*

⁵ *Istituto di Geoscienze e Georisorse, CNR, 10125 Torino, Italy*

⁶ *Dipartimento di Scienze Cliniche e Biologiche, Università di Torino, 10126 Torino, Italy*

ABSTRACT

Welding operations originate micro and nanoparticles represented by metal oxides, unoxidized metals and compounds, such as fluorides and chlorides. Welding fumes exposure is associated to lung cancer, chronic bronchitis, asthma and early Parkinson disease. Ultrafine (nanosized) particles in welding fumes are considered a risk factor in terms of occupational exposure: when inhaled, they are efficiently deposited in all regions of the respiratory tract and can translocate to other target organs as brain and systemic circulation. The study of nanoparticles emissions during welding can help to understand effects related also to new-engineered nanoparticles exposure.

In our study two real sources of Gas Tungsten Arc Welding (GTAW) fume particles, collected in an automotive plant, were characterized by means of a transmission electron microscope coupled with an energy-dispersive X-ray analytical system (TEM-EDS) and compared to a zone of the plant far from the two sources used as a reference background. The particles sampled during the automatic GTAW process were mainly constituted by iron/manganese oxide with a mean diameter of 47 nm, followed by smaller iron oxide nanoparticles (21 nm). During the manual welding process mostly aggregates with larger diameters that showed an X-ray spectrum characteristic of different kinds of silicates were found. Iron and cobalt oxides nanoparticles were present only inside bigger aggregates mainly composed of aluminum and titanium oxides.

This study confirms that welders are exposed to nano- and submicron particles and that iron/manganese oxide nanoparticles are the most representative in automatic process, despite the low concentration of manganese in welding wires (1–2%). Our results help to understand hazard related to welding fumes exposure and possible effects of nanoparticles on lung, brain and systemic circulation.

Keywords: Welding fumes; GTAW; Nanoparticles; TEM-EDS; Occupational exposure.

INTRODUCTION

In the working environment, several sources of metal nanoparticles with relevant toxicological effects can be found. Among these sources, the welding fumes are probably the most interesting one both from a chemical and toxicological point of view (Berlinger *et al.*, 2008). The high temperatures used in welding operations originate fine and

ultrafine particles represented by metal oxides, unoxidized metals and compounds, such as fluorides and chlorides (Konarski *et al.*, 2003a). The occupational exposure of welders to (nano)particles with high number concentrations, heterogeneous chemical composition and different reactivity properties may be high, since workers often are very close to the source (Buonanno *et al.*, 2011). Data in literature show that metal oxide NPs identified in lung tissue samples from welders are involved in the development of pulmonary inflammation (Andujar *et al.*, 2014). As reported by McNeilly and co-workers (2004), exposure to welding aerosols produces marked pro-inflammatory effects that are thought to be driven largely by transition metals undergoing redox cycling, resulting in oxidative stress.

*Corresponding author.

Tel.: +390405583996; Fax: +390405583903
E-mail address: gadami@units.it

Gas Tungsten Arc Welding (GTAW) is the most important technique in terms of occupational exposure because it causes the formation of smaller nanoparticles compared with other welding techniques (Lehnert *et al.*, 2012; Brand *et al.*, 2013; Miettinen *et al.*, 2016). In addition, GTAW welding has become one of the most popular welding methods in various industrial settings as the automotive one (Buonanno *et al.*, 2011) because, as reported by Kou (2003), this technique grants the operator greater control over the weld than other welding processes, allowing for very clean, strong and higher quality welds.

According to the mechanism of their formation, welding fume particles can be divided in three categories: (i) ultrafine particles (diameter < 0.1 μm), also called primary particles, formed by condensation from the gas phase; (ii) particles (diameter between 0.1 and 1 μm) which are mainly agglomerates, that are those particles made up of primary particles that adhere together because of electrostatic or van der Waals forces, and aggregates that are clumps of primary particles that have fused together; and (iii) coarse fume particles (diameter > 1 μm) formed by mechanical forces (Jenkins and Eagar, 2005).

A number of health problems are attributed to occupational exposure to welding fumes such as metal fume fever, chronic bronchitis, asthma, lung cancer and manganism (Antonini, 2003). Ultrafine particles in welding fumes are considered as a risk factor because they are characterized by a large surface-to-volume ratio. In contrast to larger-sized particles, ultrafine particles, when inhaled, are efficiently deposited in all regions of the respiratory tract and, evading specific defense mechanisms, they can translocate out of the respiratory tract and reach blood circulation and other internal organ or central nervous system via nose route causing an increase in cardiovascular diseases and neurological effects (Oberdörster *et al.*, 2005).

Characterizing dimensions, shape and composition of welding fume particles is important to better understand their toxicity and helps to clarify the possible effects of engineered nanoparticles. The comparison with known exposures, such as to welding fumes, permits to bridge effects from traditional to new “nano” exposure.

A transmission electron microscope coupled with an energy-dispersive X-ray analytical system (TEM-EDS) is an effective tool for the analysis of aerosol particles. It can provide detailed morphochemical characterization (size distributions, shapes, microchemical data and structural information) of welding fume particles.

Even if various methods have been proposed for direct and indirect particle collection on TEM grids, such as thermophoretic precipitation (Bang *et al.*, 2003), electrostatic precipitation (Miller *et al.*, 2010), and deposition onto a TEM grid of a dissolved part of the filter used to collect the particles (Moroni and Viti, 2009), the most used direct method for sampling welding fume particles on TEM grids involves impactors (cascade and electrical low pressure impactors).

At the moment, few studies have investigated the fumes at the nanometric scale and most of them are focused on gas metal arc welding (GMAW), shielded metal arc welding

(SMAW), and flux-cored arc welding (FCAW) fumes, while few studies focus on the gas tungsten arc welding (GTAW) fumes (Zimmer and Biswas, 2001; Konarski *et al.*, 2003a, b; Jenkins and Eagar, 2005; Jenkins *et al.*, 2005; Sowards *et al.*, 2008a, b; Moroni and Viti, 2009; Sowards *et al.*, 2010; Lehnert *et al.*, 2012).

The particle size distribution, morphology and chemical composition of the welding fume particles seem to be related to the welding process typology and the welding alloy (Zimmer and Biswas, 2001). An interesting study of Lehnert *et al.* (2012) found that GTAW generated smaller particles than GMAW, FCAW, and SMAW which generated mainly agglomerates with higher dimensions. The highest mass concentrations were found in FCAW, followed by GMAW and SMAW, whereas mass concentrations for GTAW were frequently not determinable because too low to be detected by weighing filter samples. Although GTAW appeared with the lowest concentrations in terms of particle mass, larger numbers of small-sized particles, including ultrafine particles, were observed. Brand *et al.* (2013) reported that GTAW generates a majority of particles at the nanoscale.

Since few studies focus on GTAW fumes particles, even though they are potentially the most hazardous ones in terms of occupational exposure, in this study two different real sources of GTAW fumes particles, collected in an automotive plant, were characterized by means of TEM-EDS and compared to a zone of the plant far from the two sources used as a reference background.

MATERIALS AND METHODS

Chemicals

All chemicals were ultrapure grade. Nitric acid ($\geq 69\%$), hydrochloric acid ($\geq 37\%$) and hydrofluoric acid (48%) were purchased from Sigma Aldrich (Milan, Italy). Water reagent grade was produced with a Millipore purification pack system (MilliQ[®] water).

Fume Collection Procedure

The welding fumes produced during the GTAW process were sampled in a factory operating in the automotive sector. Three indoor sampling zones were set (see Fig. 1): (i) in proximity of the automatic welder arm (A-GTAW); (ii) next to the operator performing manual welding (M-GTAW); (iii) in a zone of the factory approximately 500 m far from the exposure source, near the offices, used as a reference background (BKD).

In each sampling zone, at a distance of 0.5 m to the welding arc for A-GTAW and M-GTAW zones, three air sampler pumps (GilAir Plus, Sensidyne) were set to a flow of 2.2 L min⁻¹ and connected each one to a personal SKC Plastic Cyclone sampler (model no. 225-69) for respirable dust (50% cut point for 4 μm aerodynamic diameter if set to a flow rate of 2.2 L min⁻¹) containing two TEM supports (200 mesh copper grids coated with a 20 nm carbon support film, Media System Lab, Italy) to collect particles. TEM grids were placed between the filter support grid and a Mixed Cellulose Ester (MCE) filter membrane (Whatman GmbH,

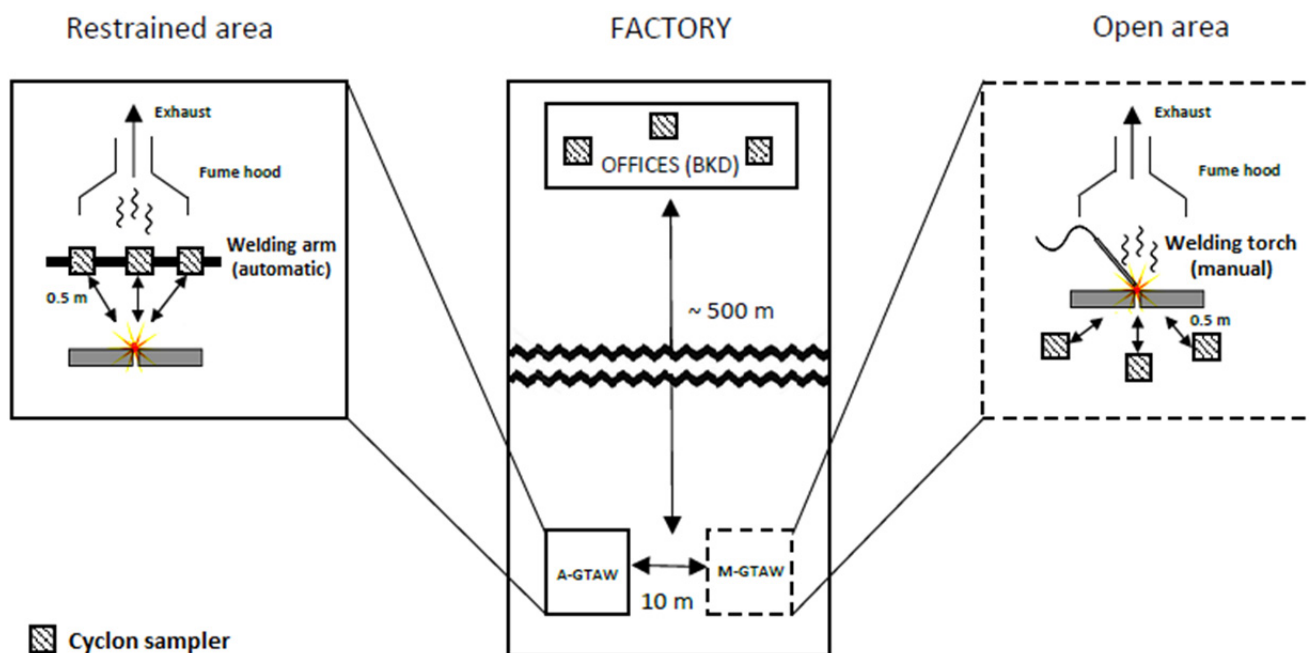


Fig. 1. Schematic representation of the sampling points in the three zones.

Germany) with 5 μm pore size for two main reasons: the first was to reduce the mobility of TEM grids due to the air flow, the second was to prevent the deposition of particles with size larger than 5 μm that could be collected by the cyclone, even if with an efficiency less than 50%, saturating the TEM grids. Therefore, in each sampling zone, six TEM grids were located. The sampling procedure lasted 20 minutes in each sampling zone.

Chemical Analysis of Welding Wires

The chemical composition of mild steel welding wires used during the automatic and manual operations was specified by the producer in the datasheet (see Table 1).

Inductively coupled plasma atomic emission spectroscopy (ICP-AES) was used to verify the chemical composition of wires. The instrument used for analysis was a PerkinElmer Optima 8000 equipped with autosampler S10.

Three independent pieces of each type of welding wire were taken from the batch used during the sampling of fumes.

A mixture of acids 1:3 (v/v) HNO_3 : HCl and HF was added to about 40 mg (5 mm) of each welding wire sample, heated till complete dissolution, then diluted to 25 mL with MilliQ

water. The obtained solutions were analyzed for total iron, manganese, silicon, chromium and copper concentration. Analyses were conducted using a calibration curve, obtained by dilution (range: 0–10 mg L^{-1}) of iron, manganese, silicon, chromium and copper standard solutions for ICP-AES analyses. The limit of detection (LOD) at the operative wavelength for each element was: 0.020 mg L^{-1} for Fe at 238.204 nm, 0.020 mg L^{-1} for Mn at 257.610 nm, 0.050 mg L^{-1} for Si at 251.611 nm, 0.050 mg L^{-1} for Cr at 267.716, 0.020 mg L^{-1} for Cu at 327.393 nm. The precision of the measurements as relative standard deviation (RSD%) was always less than 5%.

TEM-EDS Investigations

The morphological characteristics, dimensions, crystallinity and chemical composition of the particles were acquired by using a transmission electron microscope (TEM Philips CM12) working at 120 kV, equipped with LaB_6 cathode, double tilt holder, and a 622 SC CDD YAG Gatan Camera, coupled with an energy dispersive X-ray analyzer (EDS, EDAX Genesis 2000, Si(Li) detector, TEM QUANT software). The chemical data were processed with the TEM QUANT software system using default K factors.

Two TEM grids for each of the three personal cyclone samplers placed in each of the three sampling zones, for a total amount of eighteen, were investigated by means of TEM.

During TEM grids observation, dimensions of individual particles and aggregation states (agglomerates and aggregates) were collected, for a total amount of more than 750 data. As regards the identification of the aggregation state, in the agglomerates the boundaries between primary particles that form the agglomerate are clearly distinguishable in TEM images while aggregates are clumps of primary particles that have fused together and for this reason their outlines are

Table 1. Chemical composition of welding wires used during the automatic and manual operations as specified in the datasheet and verified by means of ICP-AES analysis.

Wire	% Fe	% Mn	% Si	% Cr	% Cu
Datasheet					
A-GTAW	> 90	1–2	< 1	< 0.5	< 0.5
M-GTAW	> 90	1–2	< 1	n.d.	n.d.
ICP-AES analysis					
A-GTAW	97.87	1.45	0.44	0.05	0.10
M-GTAW	96.85	1.70	0.66	0.03	0.02

n.d. = not determined.

not clearly defined. TEM images were developed only for the most significant observations and, in that case, the dimensions of particles, agglomerates and aggregates were measured by means of a Vernier scale (without an image processing tool). At the same time, over 500 EDS chemical analyses were performed. Compositional data and morphological shapes were used to identify the compound type. Besides, the obtained EDS spectra were compared with an EDS/SEM database previously made by using samples characterized in detail by other techniques (Fornero *et al.*, 2009).

Data analysis was performed using Excel (Microsoft Office Professional Plus 2010).

In this study the particles observed were grouped according to the chemical composition and aggregation state.

RESULTS

Results of Chemical Analysis of Welding Wires

The results of ICP-AES analysis confirmed the chemical composition of welding wires written in the datasheet as reported in Table 1.

Results of TEM-EDS Investigations

During TEM-EDS investigations, the chemical composition of the grid must be taken into account. The characteristic peaks due to the material of the grid (C, Cu, Ni and Zn) will be present in each acquired spectra. Sometimes, when the chemical analysis was performed close to border of the grid, a Pt peak due to X-ray emissions from microscope diaphragm appeared. A typical energy dispersive X-ray spectrum of the background of the grid in the case study is reported in Fig. 2.

A part from the peaks related to the elements that compose the material of the grids, a typical spectrum of the background of the grid showed the peaks related to O and Si. It revealed the presence of silica that was ubiquitous in all the grids collected after the fumes sampling procedure, whereas the signals of O and Si were absent in a typical spectrum of a TEM grid not exposed to the fumes.

The particles observed were grouped according to their chemical composition (Table 2) because of its significance from an occupational exposure point of view: metal oxides like iron, manganese, cobalt, titanium, aluminum and

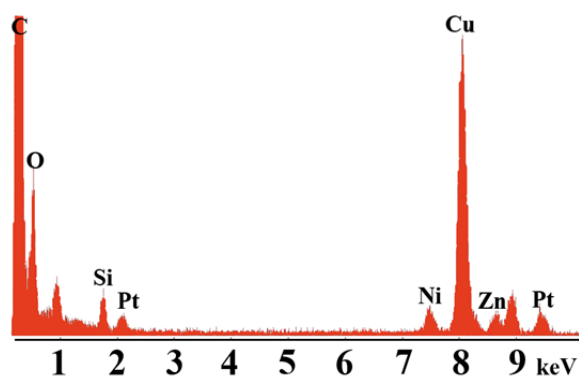


Fig. 2. Typical EDS spectrum of the background of TEM grids in the case study.

Table 2. Characterization of the particles found on A-GTAW, M-GTAW and BKD samples.

Chemical elements	Aggregation state	Minimum diameter* (µm)	Maximum diameter* (µm)	Average diameter* (µm) (SD)	Number of particles observed
A-GTAW					
O, Fe, Mn	Agglomerates of particles chainlike	0.014	0.208	0.047 (0.034)	305
O, Fe	Agglomerates of particles chainlike	0.008	0.043	0.021 (0.016)	242
O, Cr	Particles	1.250	1.292	1.276 (0.013)	13
O, Si, (Al, Mg, Fe, K, Na, Ca)	Particles, agglomerates, aggregates	0.230	1.523	0.791 (0.543)	38
M-GTAW					
O, Al, Ti	Super-aggregate	0.317	0.405	0.349 (0.035)	12
O, Fe, Co	Particles in the super-aggregates	0.008	0.061	0.022 (0.015)	51
O, Cr	Aggregates	0.531	2.621	1.434 (0.716)	17
O, Si, (Al, Mg, Fe, K, Na, Ca)	Aggregates	0.328	1.752	0.924 (0.527)	32
BKD					
O, Si, (Al, Mg, Fe)	Particles, agglomerates, aggregates	0.036	2.016	0.537 (0.626)	43

Note: Chemical composition, aggregation state and dimensions revealed by TEM-EDS investigations for automatic and manual gas tungsten arc welding (A-GTAW, M-GTAW) samples and samples collected far from the welding fumes source (BKD). The list of main chemical elements is indicated in decreasing abundance order.
* Feret diameter.

chromium oxides, and silicates. Silica particles have been demonstrated to persist in the lungs, and this greater pulmonary persistence may contribute to the chronic lung disease (silicosis) that it causes (Brody *et al.*, 1982). From literature it is also known that welding related nanoparticles (as iron, chromium, and manganese oxides) could be responsible, at least in part, for the pulmonary inflammation observed in welders (Andujar *et al.*, 2014).

On the grids collected in the zone in which automatic welding was performed (A-GTAW), particles, agglomerates and aggregates of a wide dimensional range were observed. The most representative particles were constituted by iron/manganese oxide. Nanoparticles with this chemical composition formed agglomerates chainlike as shown in Figs. 3 and 4. The equivalent diameter (Feret diameter) (Merkus, 2009) of about 300 particles was measured and the

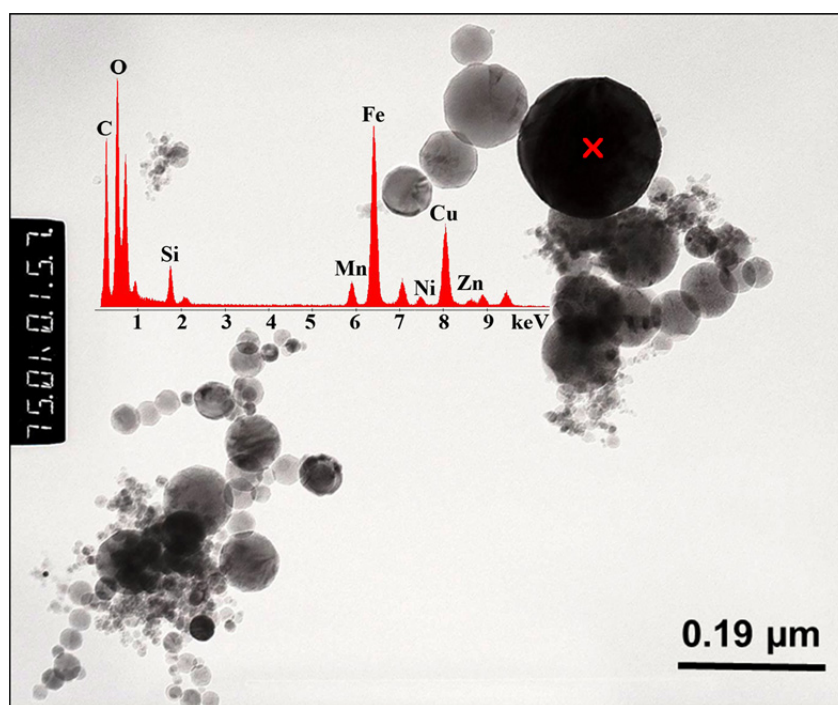


Fig. 3. Representative TEM image and EDS spectrum of an agglomerate found on a A-GTAW sample. Note: Scale bar: 0.19 μm. The colored X in figure represents the center of the microanalysis spot. Spectrum refers to iron/manganese oxide.

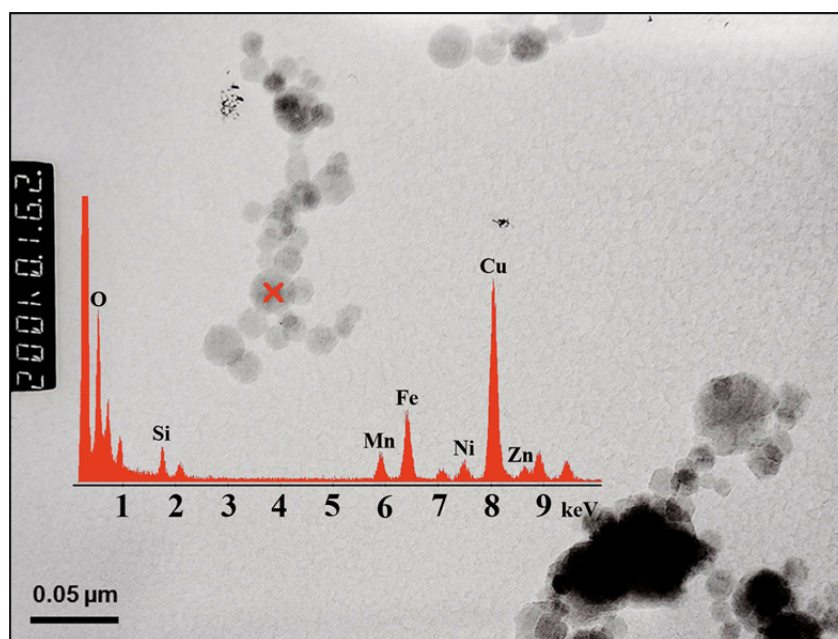


Fig. 4. Representative TEM image and EDS spectrum of an agglomerate found on a A-GTAW sample. Note: Scale bar: 50 nm. The colored X in figure represents the center of the microanalysis spot. Spectrum refers to iron/manganese oxide.

average diameter was 47 nm. The second more represented group in grids was agglomerates of iron oxide nanoparticles chainlike (Fig. 5) with a mean diameter of 21 nm. Very few are chromium oxide single particles with an average diameter of 1.276 μm . Agglomerates and aggregates of different kinds of silicates were found with average diameter of 0.791 μm .

On the grids collected in the zone in which manual welding was performed (M-GTAW), three kinds of aggregates were observed. Fig. 6 shows an example of the first kind of

super-aggregates, mainly composed of aluminum and titanium oxides (X-ray spectrum in blue), with an average diameter of 0.349 μm . Inside these super-aggregates some iron and cobalt oxides nanoparticles (X-ray spectrum in red) with an average diameter of 22 nm were observed. The second kind of aggregates (Figs. 7 and 8) was composed of chromium oxides and had an average diameter of 1.434 μm . The third kind of aggregates had an average diameter of 0.924 μm and showed an X-ray spectrum characteristic of different kinds of silicates.

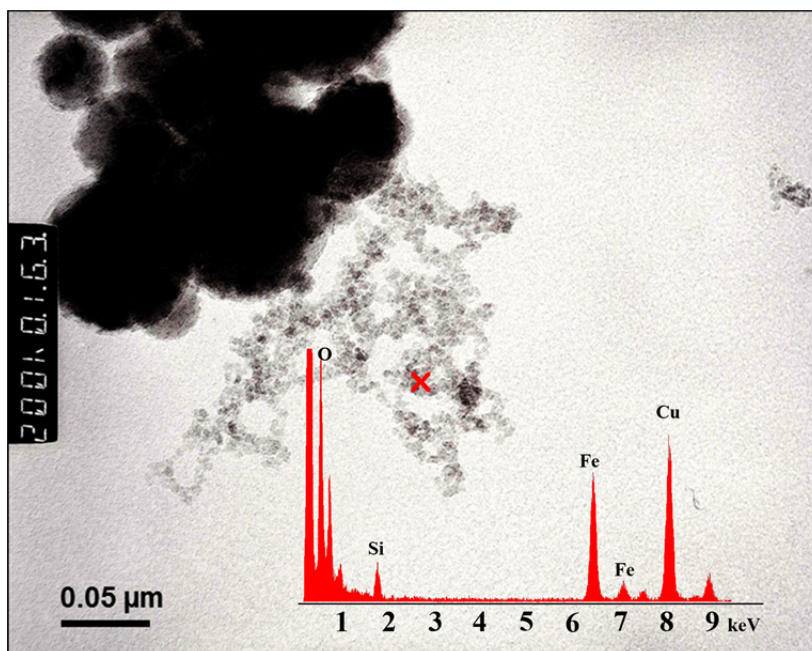


Fig. 5. Representative TEM image and EDS spectrum of an agglomerate found on a A-GTAW sample. Note: Scale bar: 50 nm. The colored X in figure represents the center of the microanalysis spot. Spectrum refers to iron oxide.

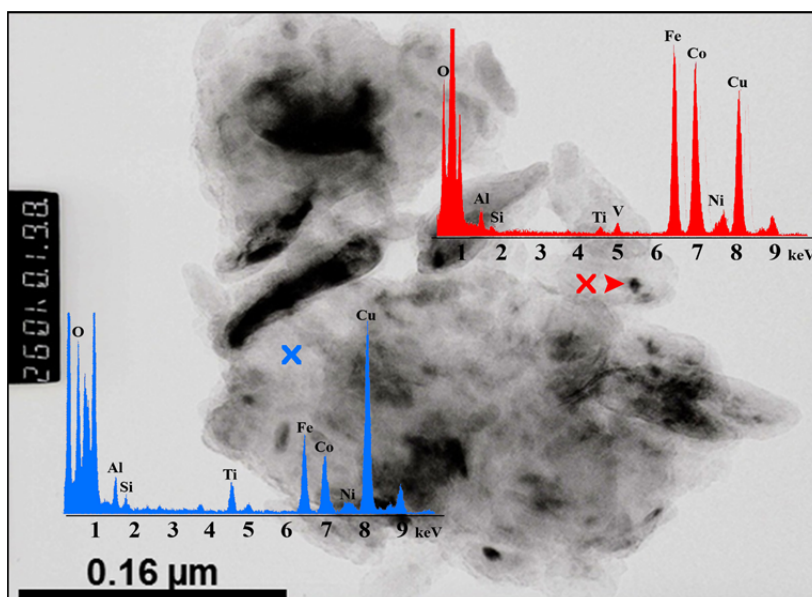


Fig. 6. Representative TEM image and EDS spectra of a super-aggregate found on an M-GTAW sample. Note: Scale bar: 0.16 μm . The colored X in figure represent the centers of the microanalysis spot. Red spectrum refers to iron and cobalt oxides, the blue one refers to aluminum and titanium oxides.

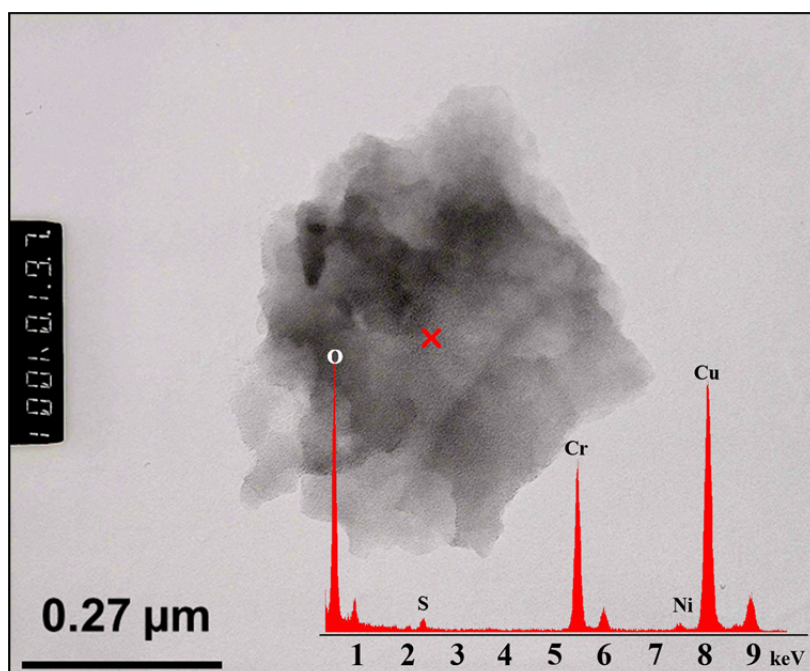


Fig. 7. Representative TEM image and EDS spectrum of an aggregate found on a M-GTAW sample. Note: Scale bar: 0.27 μm . The colored X in figure represents the center of the microanalysis spot. Spectrum refers to chromium oxide.

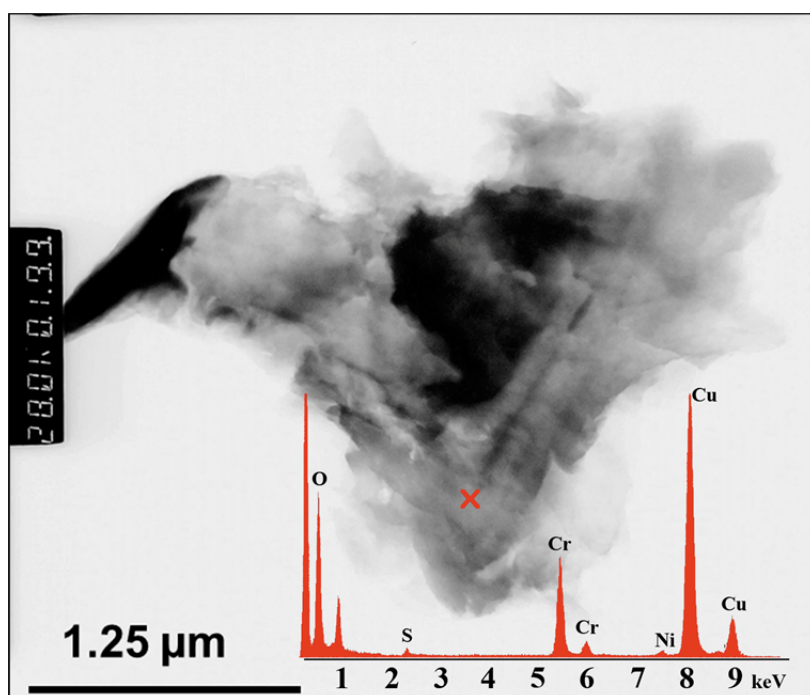


Fig. 8. Representative TEM image and EDS spectrum of an aggregate found on a M-GTAW sample. Note: Scale bar: 1.25 μm . The colored X in figure represents the center of the microanalysis spot. Spectrum refers to chromium oxide.

On the grids collected in the zone far from the welding fumes source (BKD), particles, agglomerates and aggregates were found. Figs. 9 and 10 show two examples of aggregates that were probably aluminosilicates (Fig. 9) and phyllosilicates (Fig. 10), amorphous and in some cases crystalline. The average diameter of these particles was 0.537 μm .

DISCUSSION

During the GTAW process the aerosol generated is mainly nanosized: Miettinen *et al.* (2016) reported a geometric mean diameter of 46 nm in the middle of the workshop and lower size near the breathing zone. Similar results were found by Berlinger *et al.* (2011), Lehnert *et al.* (2012) and

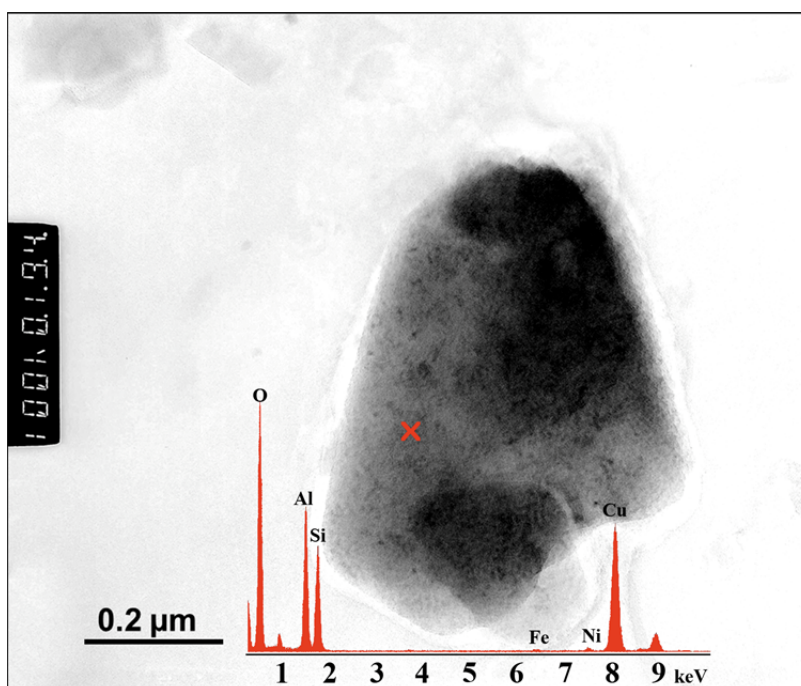


Fig. 9. Representative TEM image and EDS spectrum of an aggregate found on a BKD sample. Note: Scale bar: 0.20 μm . The colored X in figure represents the center of the microanalysis spot. Spectrum refers to an alluminosilicate.

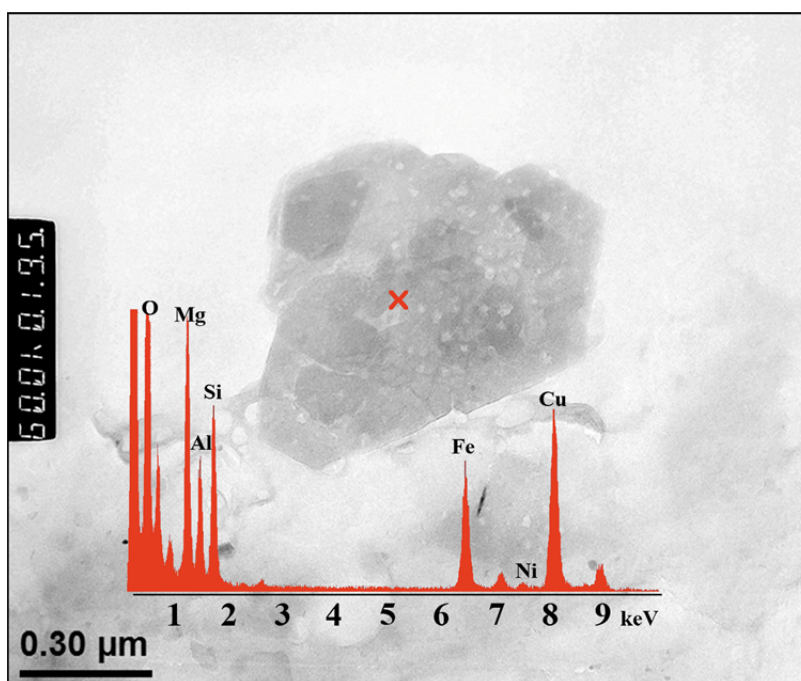


Fig. 10. Representative TEM image and EDS spectrum of an aggregate found on a BKD sample. Note: Scale bar: 0.30 μm . The colored X in figure represents the center of the microanalysis spot. Spectrum refers to a phyllosilicate.

Brand *et al.* (2013). In our study we went deeply on shape and chemical composition of nano- and submicron particles emitted during both automatic and manual GTAW of steel to clarify their characteristics, finding new data that can help to understand the link between exposure and toxicity for exposed workers.

Analyzing automatic GTAW, TEM observations of size

and shape of the collected particles are substantially in agreement with previous studies (Berlinger *et al.*, 2011; Graczyk *et al.*, 2016). No individual primary particles in the nanoscale were found. Particles in the ultrafine range were predominantly spherical, in some cases polyhedral, with clearly distinguishable boundaries and formed chainlike agglomerates with fractal geometry. The majority of emitted

particles in respirable range was chainlike agglomerates constituted by iron/manganese oxide nanoparticles with size ranging from 14 to 208 nm and a mean value of 47 nm. Despite the low percentage of manganese in wires (< 2%), the smallest then more dangerous particles emitted during the welding process contained manganese. About the 90% of iron/manganese oxide particles observed was smaller than 100 nm: about 67% were in the range 0–50 nm, 24% in the range 50–100 nm, only 9% in the range 100–210 nm.

This result is highly significant from a toxicological point of view: it is possible that, after inhalation, the van der Waals and electrostatic forces holding agglomerates together are at least partially disrupted, breaking agglomerates into their primary particle constituents or smaller agglomerates (Richman *et al.*, 2011). It is already reported in literature (Zimmer *et al.*, 2002) that the arc welding activities represent a source of exposure to high amounts of fumes containing manganese, also in nanoparticle size. From a study population of welders, Racette *et al.* (2001) showed that some of them would develop Parkinsonism 17 years earlier compared to the general population, thus placing the problem of understanding what was the penetration pathway of the metal into the inner brain structures and, in particular, inside the basal nuclei, the central nervous system regions most involved in the genesis of the disease. In nano-form this metal can translocate through the olfactory tract reaching the brain, where it can cause a neurological disease called manganism, with Parkinson-like symptoms (Yu *et al.*, 2000; McMillian, 2005).

Manganese enrichment in A-GTAW samples, if compared to M-GTAW ones, is in agreement with Moroni and Viti (2009) and Jenkins (2003) who report that it is a function of decreasing of magnetite-like particles size in welding fumes. For this reason, even if the time of direct exposure of workers to the fumes generated during the automatic process in the restrained area is brief, an effective local exhaust ventilation is necessary.

Another metal, that can have an important role in lung toxicity, is chromium, but in the case of automatic GTAW the size of chromium particles is higher reaching an average diameter of 1.276 μm . No chromium nanoparticles were found in aerosol sampled during the welding process.

In manual GTAW the pattern of particles changed: particles observed on TEM grids were mostly amorphous and irregular-shaped aggregates. In some cases, these aggregates seem to be formed by thin and irregular plate-like particles overlapped and fuse together. The most representative nanoparticles were constituted by iron/cobalt oxide, with an average diameter of 22 nm, that were present inside aggregates of higher dimensions. As in the automatic welding, chromium was present only in bigger aggregates while no manganese oxide nanoparticles were found on TEM grids.

In our study particles, agglomerates and aggregates composed of silicates were ubiquitous. On all collected TEM grids no fibres were found. The presence of silicates on A-GTAW and M-GTAW samples reflects in part the chemical composition of the welding wires (silicon was a component of the two kinds of wires), in part is due to the

atmospheric particulate matter of natural origin that was found also in BKD samples. Aluminosilicates and phyllosilicates are widely used for example in constructions materials like plasters and paints. The fact that in BKD samples metal oxides particles, like iron, manganese, cobalt and chromium oxides, were not observed, confirms that the source of metal oxides was only the welding process.

Particles produced in both welding processes (automatic and manual) are respirable according to ISO-CEN (Organization for Standardization - European Committee for standardization) definition (CEN, 1993) but the most significant difference between the two sources of welding fumes that were investigated is the aggregation state of the particles found on TEM grids. The particles sampled during the automatic process had the smallest diameter in comparison with those sampled in the M-GTAW zone, were mostly nanosized and formed agglomerates chainlike. The particles found in the M-GTAW zone, instead, showed a larger diameter and were mostly aggregates. These results generate the hypothesis that even the same kind of welding process produces different classes of particles depending on the lifetime of the welding process. As a matter of fact, the automatic welding is a fast process in which the contact between the tungsten electrode, the filler wire and the material that has to be welded is brief. On the other hand, the automatic welding is performed inside a restrained area that workers cannot enter until the end of the welding process when they pick up the welded pieces to complete and refine them manually. In the manual process the fume was generated by the welder who completed and refined the pieces treated in the automatic process (the operator welds a defined spot for a longer period of time respect to the automatic welding arm).

Our results on size and morphology of M-GTAW particles seem to be in contrast with Graczyk *et al.* (2016) who conducted the exposure assessment of apprentice welders during aluminum manual GTAW in a ventilated exposure cabin to have a controlled setting. As regards particle size distribution evaluated by means of particle sizers, they reported that at the breathing zone, 92% of the particles had a geometric mean diameter below 100 nm and 50% of the particles was below 41 nm. Moreover, particles collected on TEM grids formed chainlike agglomerates of primary particles in the nanoscale.

On the contrary, in M-GTAW zone of our study we found mostly aggregate of particles that were not in the nanoscale. These differences can be due to the prevalence of the accumulation over the nucleation mechanism of particle formation and the influence of other industrial processes during our manual welding activity that was not performed in a controlled setting. In these terms, our results are substantially in agreement with Moroni and Viti (2009) who characterized GMAW fumes and pointed out the differences in aerosol composition in terms of particle size at variable distances from the welding chambers. The influence of the industrial setting resulted in greater particle size variability and larger particle size of welding fumes compared to a controlled (laboratory) and/or confined setting. Moreover, Dasch and D'Arcy (2008) reported a

size distribution mode for aluminum GMAW fumes in an automotive plant at 0.8 μm compared to 0.2–0.4 reported in literature for controlled settings.

For what concern the risk assessment during M-GTAW, we have to notice that our sampling was performed at a distance of 0.5 m away from the welding task, not in the breathing zone where the particle number concentration could be actually higher as reported by Graczyk *et al.* (2016) who found that the mean particle number concentration at the breathing zone (inside the welding helmet) was 54% higher ($1.69\text{E}+06$ particles cm^{-3}) than at the near field location (0.6 m away from the welding task) confirming that the exposure increases with the decrease of the distance from the source and that a non-ventilated welding helmet is not a sufficient protection measure. For this reason, also the particle number concentration, not only particle size and morphology, have to be taken into account during manual welding.

CONCLUSIONS

Characterizing dimensions, shape and composition of welding fume particles is important to better understand how they can originate occupational diseases in welders with special attention to ultrafine particles.

Since in literature there are few studies that focus on GTAW fumes particles even though they are potentially the most hazardous ones in terms of occupational exposure, in this study two different real sources of GTAW fumes particles, collected in an automotive plant, were characterized by means of TEM-EDS and compared to a zone of the plant far from the two sources, used as a reference background.

All particles observed in this study are in the class of respirable particulate matter. The particles sampled during the automatic welding process had the smallest diameter in comparison with those sampled in the M-GTAW zone, were mostly nanosized, constituted by iron/manganese oxide and formed chainlike agglomerates. The particles found in the M-GTAW zone, instead, showed a larger diameter and were mostly aggregates that showed an X-ray spectrum characteristic of different kinds of silicates. Iron and cobalt oxides nanoparticles were present only inside bigger aggregates mainly composed of aluminum and titanium oxides.

These results generate the hypothesis that even the same kind of welding process produces different classes of particles depending on factors like the lifetime of the welding process. It was also demonstrated that chemical composition of the particles reflected the composition of the mild steel used during the welding processes, meanwhile only particulate matter correlated to the building construction (as plaster) was found in BKD samples.

ACKNOWLEDGMENTS

This work was supported by the Commissariato del Governo nella Regione Friuli Venezia Giulia that provided doctoral research funding (“Fondo Trieste”) to EBe.

AUTHORS' CONTRIBUTIONS

The study was planned by FL and GA with contribution from MC and CB. CB and GM managed and performed the sampling procedure. CB, EBa, EBe and SC performed TEM-EDS investigations and EBa and MC performed ICP-AES analyses. EBa, EBe and CB performed the data analysis. MC performed the graphic design of the manuscript. The manuscript was written by EBa, EBe and GA with contributions from all co-authors. All authors have approved the final article.

CONFLICTS OF INTEREST

The authors declare no conflict of interest.

REFERENCES

- Andujar, P., Simon-Deckers, A., Galateau-Sallé, F., Fayard, B., Beaune, G., Clin, B., Billon-Galland, M.A., Durupthy, O., Pairon, J.C., Doucet, J., Boczkowski, J. and Lanone, S. (2014). Role of metal oxide nanoparticles in histopathological changes observed in the lung of welders. *Part. Fibre Toxicol.* 11: 23–35.
- Antonini, J.M. (2003). Health effects of welding. *Crit. Rev. Toxicol.* 33: 61–103.
- Bang, J.J., Trillo, E.A. and Murr, L.E. (2003). Utilization of selected area electron diffraction patterns for characterization of air submicron particulate matter collected by a thermophoretic precipitator. *J. Air Waste Manage. Assoc.* 53: 227–236.
- Berlinger, B., Ellingsen, D.G., Naray, M., Zaray, G. and Thomassen, Y. (2008). A study of the bio-accessibility of welding fumes. *J. Environ. Monit.* 10: 1448–1453.
- Berlinger, B., Benker, N., Weinbruch, S., L'Vov, B., Ebert, M., Koch, W., Ellingsen, D.G. and Thomassen, Y. (2011). Physicochemical characterization of different welding aerosols. *Anal. Bioanal. Chem.* 399: 1773–1780.
- Brand, P., Lenz, K., Reisgen, U. and Kraus, T. (2013). Number size distribution of fine and ultrafine fume particles from various welding processes. *Ann. Occup. Hyg.* 57: 305–313.
- Brody, A.R., Roe, M.W., Evans, J.N. and Davis, G.S. (1982). Deposition and translocation of inhaled silica in rats: quantification of particle distribution, macrophage participation, and function. *Lab. Invest.* 47: 533–542.
- Buonanno, G., Morawska, L. and Stabile, L. (2011). Exposure to welding particles in automotive plants. *J. Aerosol Sci.* 42: 295–304.
- CEN. European Committee for Standardization (1993). Workplace atmospheres: size fraction definitions for measurement of airborne particles (Report No. BS EN 481:1993). London, England: CEN, British Standards Institute.
- Dasch, J. and D'Arcy, J. (2008). Physical and chemical characterization of airborne particles from welding operations in automotive plants. *J. Occup. Environ. Hyg.* 5: 444–454.
- Fornero, E., Belluso, E., Capella, S. and Bellis, D. (2009).

- Environmental exposure to asbestos and other inorganic fibres using animal lung model. *Sci. Tot. Environ.* 407: 1010–1018.
- Graczyk, H., Lewinski, N., Zhao, J., Concha-Lozano, N. and Riediker, M. (2016). Characterization of Tungsten Inert Gas (TIG) welding fume generated by apprentice welders. *Ann. Occup. Hyg.* 60: 205–219.
- Jenkins, N.T. (2003). *Chemistry of airborne particles from metallurgical processing*. Ph.D. thesis, Massachusetts Institute of Technology, pp.189.
- Jenkins, N.T. and Eagar, T.W. (2005). Chemical analysis of welding fume particles. *Weld. J.* 84: 87s–93s.
- Jenkins, N.T., Pierce, W.M. and Eagar, T.W. (2005). Particle size distribution of gas metal and flux cored arc welding fumes. *Weld. J.* 84: 156–163.
- Konarski, P., Iwanejko, I. and Ćwil, M. (2003a). Core-shell morphology of welding fume micro- and nanoparticles. *Vacuum* 70: 385–389.
- Konarski, P., Iwanejko, I. and Mierzejewska, A. (2003b). SIMS depth profiling of working environment nanoparticles. *Appl. Surf. Sci.* 203–204: 757–761.
- Kou, S. (2003). *Welding metallurgy*. 2nd edn, Wiley & Sons Inc, London
- Lehnert, M., Pesch, B., Lotz, A., Pelzer, J., Kendzia, B., Gawrych, K., Heinze, E., Van Gelder, R., Punkenburg, E., Weiss, T., Mattenklott, M., Hahn, J.U., Möhlmann, C., Berges, M., Hartwig, A. and Brüning, T. (2012). Exposure to inhalable, respirable, and ultrafine particles in welding fumes. *Ann. Occup. Hyg.* 56: 557–567.
- McMillan, G. (2005). Is electric arc welding linked to manganese or Parkinson's disease? *Toxicol. Rev.* 24: 237–257.
- Merkus, H.G. (2009). *Particle size measurements: Fundamentals, practice, quality*, Springer.
- McNeilly, J.D., Heal, M.R., Beverland, I.J., Howe, A., Gibson, M.D., Hibbs, L.R., MacNee, W. and Donaldson, K. (2004). Soluble transition metals cause the pro-inflammatory effects of welding fumes in vitro. *Toxicol. Appl. Pharmacol.* 196: 95–107.
- Miettinen, M., Torvela, T. and Leskinen, J.T. (2016). Physicochemical characterization of aerosol generated in the gas tungsten arc welding of stainless steel. *Ann. Occup. Hyg.* 60: 960–968.
- Miller, A., Frey, G., King, G. and Sunderman, C. (2010). A handheld electrostatic precipitator for sampling airborne particles and nanoparticles. *Aerosol Sci. Technol.* 44: 417–427.
- Moroni, B. and Viti, C. (2009). Grain size, chemistry, and structure of fine and ultrafine particles in stainless steel welding fumes. *J. Aerosol Sci.* 40: 938–949.
- Oberdörster, G., Oberdörster, E. and Oberdörster, J. (2005). Nanotoxicology: An emerging discipline evolving from studies of ultrafine particles. *Environ. Health Perspect.* 113: 823–839.
- Racette, B.A., McGee-Minnich, L., Moerlein, S.M., Mink, J.W., Videen, T.O. and Perlmutter, J.S. (2001). Welding-related parkinsonism. Clinical features, treatment, and pathophysiology. *Neurology* 56: 8–13.
- Richman, J.D., Livi, K.J.T. and Geyh, A.S. (2011). A scanning transmission electron microscopy method for determination of manganese composition in welding fume as a function of primary particle size. *J. Aerosol Sci.* 42: 408–418.
- Sowards, J.W., Ramirez, A.J., Lippold, J.C. and Dickinson, D.W. (2008a). Characterization procedure for the analysis of arc welding fume. *Weld. J.* 87: 76–83.
- Sowards, J.W., Lippold, J.C., Dickinson, D.W. and Ramirez, A.J. (2008b). Characterization of welding fume from SMAW electrodes – Part I. *Weld. J.* 87: 106–112.
- Sowards, J.W., Ramirez, A.J., Dickinson, D.W. and Lippold, J.C. (2010). Characterization of welding fume from SMAW electrodes – Part II. *Weld. J.* 89: 82–90.
- Yu, I.J., Kim, K.J., Chang, H.K., Song, K.S., Han, K.T., Han, J.H., Maeng, S.H., Chung, Y.H., Park, S.H., Chung, K.H., Han, J.S. and Chung, H.K. (2000). Pattern of deposition of stainless steel welding fume particles inhaled into the respiratory systems of Sprague-Dawley rats exposed to a novel welding fume generating system. *Toxicol. Lett.* 116: 103–111.
- Zimmer, A. T. and Biswas, P. (2001). Characterization of the aerosols resulting from arc welding processes. *J. Aerosol Sci.* 32: 993–1008.
- Zimmer, A.T., Baron, P.A. and Biswas, P. (2002). The influence of operating parameters on number-weighted aerosol size distribution generated from a gas metal arc welding process. *J. Aerosol Sci.* 33: 519–531.

Received for review, July 9, 2017

Revised, September 13, 2017

Accepted, October 18, 2017